Optimal ATMS Remapping Algorithm for Climate Research

Hu Yang, *Member, IEEE*, and Xiaolei Zou

***Abstract*—In this paper, the Backus–Gilbert (B–G) method was used for the conversion from Advanced Technology Microwave Sounder (ATMS) FOVs to AMSU-A FOVs. This method provides not only an optimal combination of measurements within a specified region but also a quantitative measure of the tradeoff between resolution and noise. Based on a subpixel microwave antenna temperature simulation technique, ATMS observations at a specified FOV size with 1.1° sampling interval are simulated. Errors of remapping results were quantified by using simulated data sets and real AMSU observations. It is shown that the biases and/or standard deviations of brightness temperatures are significantly reduced by using the B–G generated remapping coefficients. For K/Ka bands, a resolution enhancement by the remap of ATMS observations introduces about 0.6 K increase in noise. For other bands, the channel sensitivity was improved for the remapped data.**

***Index Terms*—Advanced Microwave Sounding Unit (AMSU), Advanced Technology Microwave Sounder (ATMS), remapping.**

I. Introduction

THE Advanced Technology Microwave Sounder (ATMS) is a total power cross-track scanning microwave radiometer with 22 channels located from 23 to 183 GHz. It provides temperature sounding information in the troposphere and stratosphere (i.e., from the surface to about 1 kPa or 45 km) and humidity sounding information in the troposphere (i.e., from the surface to about 200 kPa or 15 km) [1]. From the ATMS 22 channels, 17 ATMS channels (e.g., channels 1–3, 5–15,18, 20, and 22) have the same frequencies as its predecessor AMSU, except for some polarization and bandwidth differences. Three new channels are added: ATMS channel 4 for temperature sounding and ATMS channels 19 and 21 for humidity sounding. There are two receiving antennas on ATMS. One antenna serves 15 channels with frequencies below 60 GHz, and the other serves the remaining seven channels with frequencies above 60 GHz. The first antenna has a beamwidth of 2.2° for channels 3–15 and 5.2° for the two lowest frequency channels 1–2 (23.8 and 31.4 GHz). The second antenna has a beamwidth of 1.1° for all six high-frequency channels 17–22 and a beamwidth of 2.2° for the lowest high-frequency channel 16 (89 GHz).

ATMS combines all the channels of its predecessors AMSU (e.g., AMSU-A1, AMSU-A2, and AMSU-B) sensors into a single package with considerable savings in mass, power, and volume. The most notable change in instrument design is the scan fashion for ATMS window and temperature sounding channels, which is different from its predecessor instrument AMSU-A. AMSU-A is designed with a stepped-scan fashion: the instrument's antenna rotates to a data collection position, stops, collects data, then moves to the next collection position, stops, collects data, etc. Thirty contiguous scene resolution cells are sampled every 8 s. The integration time for each FOV is 165 ms, which ensures an instrument sensitivity as high as 0.2–0.3 K for most channels [2]. For ATMS, in order to keep all 22 channels in the same scan mode and with the sampling time, a continuous-scan fashion is adopted. Ninety-six scene resolution cells are sampled at an interval of 8/3 s. Each scan covers 52.725° on both sides of the subsatellite path. The integration time for each FOV is only 18 ms and the sampling to have the same noise level as AMSU channels when averaged over 3×3 ATMS FOVs [3]. Short sampling time and large FOV size result in an overlapping between FOVs for ATMS K/V/W bands. Approximately, the 4/5 pixel is overlapped with its neighboring pixel for K bands and 1/2 pixel for V and W bands.

Linking ATMS to its heritage instruments AMSU-A/B is highly desirable for climate change study [4]–[7]. The oversampling characteristics of ATMS observations make it possible to map the ATMS observations into AMSU-A-like observations. In this paper, the Backus–Gilbert (B–G) method was used as an optimal remapping algorithm, which converts ATMS observations at K, V, and W bands from 5.2° and 2.2° FOV size to a consistent AMSU-A 3.3° FOV size. This method provides not only an optimal average of brightness temperatures within a specified region but also a quantitative measure of the tradeoff between resolution and noise [8]. This paper is organized as follows: The B–G algorithm is introduced in Section II, along with some detailed discussions on determining an error conditioning factor in the B–G algorithm for generating the optimal remapping coefficients. A quantitative evaluations of the remapping products were carried out for simulated data sets and real AMSU observations in Sections III and IV, respectively. Summary and conclusions are provided in Section V.

II. Description of the B–G Remapping Algorithm

The B–G algorithm can be considered as an optimum method for image rebuilt, and it was applied for spatial resolution

Manuscript received June 9, 2013; revised September 24, 2013; accepted February 18, 2014. Date of publication April 2, 2014; date of current version May 30, 2014. This work was supported in part by the Chinese Ministry of Science and Technology 973 Project under Grant 2010CB951600 and in part by the National Science Foundation under Grant 91337218.

H. Yang is with the Earth System Science Interdisciplinary Center, University of Maryland, College Park, MD 20740 USA (e-mail: huyang@umd.edu).

X. Zou is with the Department of Earth, Ocean and Atmospheric Science, Florida State University, Tallahassee, FL 32306-4520 USA.

Color versions of one or more of the figures in this paper are available online at http://ieeexplore.ieee.org.

Digital Object Identifier 10.1109/TGRS.2014.2310702

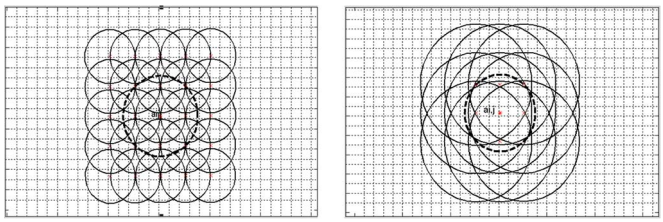

Fig. 1. Schematic illustration of the (dashed circle) expected FOV size and (solid circle) raw observations in the B–G remapping algorithm for (left) resolution reduction and (right) enhancement processes.

enhancement or reduction of observations from a spaceborne microwave imager instrument as early as 1970s by Stogryn [8]. Since then, the B–G algorithm was widely used as a remapping algorithm for single-antenna-reflector multifrequency microwave radiometers such as SSMI, TMI, AMSR-E, etc. [9]–[12]. The theory for the B–G algorithm was developed and discussed in the cited literature. Only a brief description of the B–G method is provided below. Emphasis is given to those details associated with the generation of the optimal remapping coefficients, which can be applied to real ATMS observations to obtain AMSU-A-like observations.

Fig. 1 is an illustration of what does the B–G remapping algorithm do. Fig. 1(a) is a downscaling of ATMS 2.2° FOV to AMSU 3.3° FOV size, and Fig. 1(b) is for conversion of ATMS 5.2° FOV to AMSU 3.3° FOV size. The former is a resolution reduction, and the latter is a resolution enhancement process. In Fig. 1, the solid circles are ATMS observations with the original FOV size, and the dashed circle is a constructed observation at the expected FOV size. The B–G algorithm finds a set of optimal coefficients a_{ij} for constructing a new observation $T^a(\hat{\rho}_0)$ at the location $\hat{\rho}_0$ with an expected FOV size as a linear combination of $m \times n$ numbers of adjacent original observed antenna brightness temperatures $T^a(\hat{\rho}_{ij})$ at the locations $\hat{\rho}_{ij}$, i.e.,

$$T^a(\hat{\rho}_0) = \sum_{i=1}^{n}\sum_{j=1}^{n} a_{ij} T^a(\hat{\rho}_{ij}). \tag{1}$$

Realizing that the antenna temperature $T^a(\hat{\rho}_0)$ seen by a real antenna at a location $\hat{\rho}_0$ with a certain FOV size is the convolution of actual scene brightness temperature $T^b(\hat{\rho})$ with antenna gain. In other words, $T^a(\hat{\rho}_0)$ on the left side of (1) can be also expressed as

$$T^a(\hat{\rho}_0) = \int F(\hat{\rho}_0, \hat{\rho}) T^b(\hat{\rho}) dA. \tag{2}$$

Similarly, the antenna temperatures $T^a(\hat{\rho}_{ij})$ for real observations on the right side of (1) can be written as

$$T^a(\hat{\rho}_{ij}) = \int G(\hat{\rho}_{ij}) T^b(\hat{\rho}) dA. \tag{3}$$

In the aforementioned equations, $F(\hat{\rho}_0, \hat{\rho})$ is the target antenna gain at an expected FOV size, and $G(\hat{\rho}_{ij})$ is the antenna gain at the original FOV size. Both G and F are known from ground measurements. Equations (1) and (3) can be combined to yield

$$T^a(\hat{\rho}_0) = \int \left(\sum_{i=1}^{n}\sum_{j=1}^{n} a_{ij} G_{ij}(\hat{\rho}) \right) T^b(\hat{\rho}) dA. \tag{4}$$

It should be noted that the 3-D antenna pattern is interpolated from the ground-measured antenna pattern data available only at a limited number of antenna pattern cuts with different scan angles. It is reminded that the measurement accuracy at different scan angles is different. In general, measurement accuracy in nadir is highest and will degrade with the increase in scan angle. It is also pointed out that additional errors could be introduced by the interpolation.

The B–G algorithm aims at finding a set of coefficients, a_{ij} in (4) so that the bracketed term in (4) is close to the expected gain function $F(\hat{\rho}_0, \hat{\rho})$. It also ensures that the instrument noise is not significantly increased, which is particularly important for resolution enhancement processing. Specifically, the following quantity is minimized [8]:

$$Q = Q_0 \cos\gamma + (\Delta T_{\rm rms})^2 w \sin\gamma \tag{5}$$

with

$$Q_0 = \int \left[\sum_{i=1}^{n}\sum_{j=1}^{n} a_{ij} G_{ij}(\hat{\rho}) - F(\hat{\rho}_0, \hat{\rho}) \right]^2 dA \tag{6}$$

where $\Delta T_{\rm rms}$ is the channel noise, w, and γ are adjustable scale factors described in [9]. Minimizing Q with respect to a_{ij} subject to the constraint $\int \sum_{i=1}^{n}\sum_{j=1}^{n} a_{ij} G_{ij}(\hat{\rho}) dA = 1$ shall produce the best correction coefficients possible in the least squares sense.

The details of solving for the coefficients a_{ij} can be found in [8] and [9]. The final result is as follows:

$$a = S^{-1}\left[\cos\gamma \cdot v + \left(\frac{1 - \cos\gamma \cdot u^T S^{-1} v}{u^T S^{-1} u} \right) u \right] \tag{7}$$

with

$$S = \cos\gamma \cdot G_{ij} + \delta \cdot w \cdot E \cdot \sin\gamma,\ u_i = \int G_i(\rho) dA,$$

$$v_i = \int G_i(\rho) F(\rho) dA,\ G_{ij} = \int G_i(\rho) G_j(\rho) dA$$

where δ is the Kronecker delta function, and E is NEDT in unit kelvin. Note that in the above equations, antenna gains G and F have been changed to be expressed as a 1-D function, with subscript i and j representing any two adjacent pixels.

In calculating the remapping coefficients defined by (7), three parameters must be varied to determine the optimal remapping coefficients. The first parameter is n, the total number of observations that are used to perform the correction. In this paper, $n \times n$ that is equal to 3×3, 5×5, and 7×7 is tested in the implementation of the B–G algorithm. It is found that the best data grid for obtaining the optimal remapping coefficients is dependent on the difference of FOV size between the original observations (e.g., ATMS) and the reconstructed

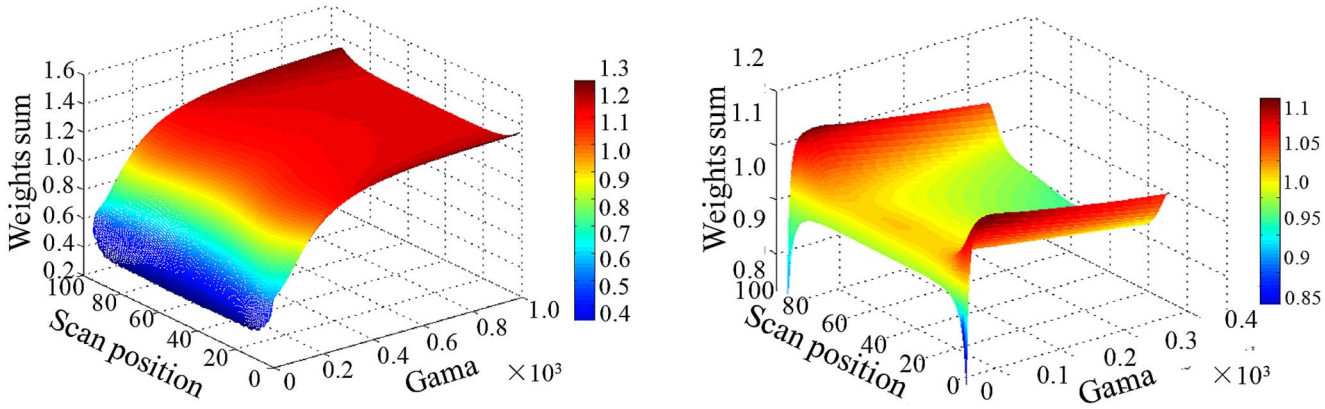

Fig. 2. Variations of the B–G remapping weight functions with respect to scan positions and γ value for the(left) conversion from 5.2° to 3.3° beamwidth and (right) conversion from 2.2° to 3.3° beamwidth.

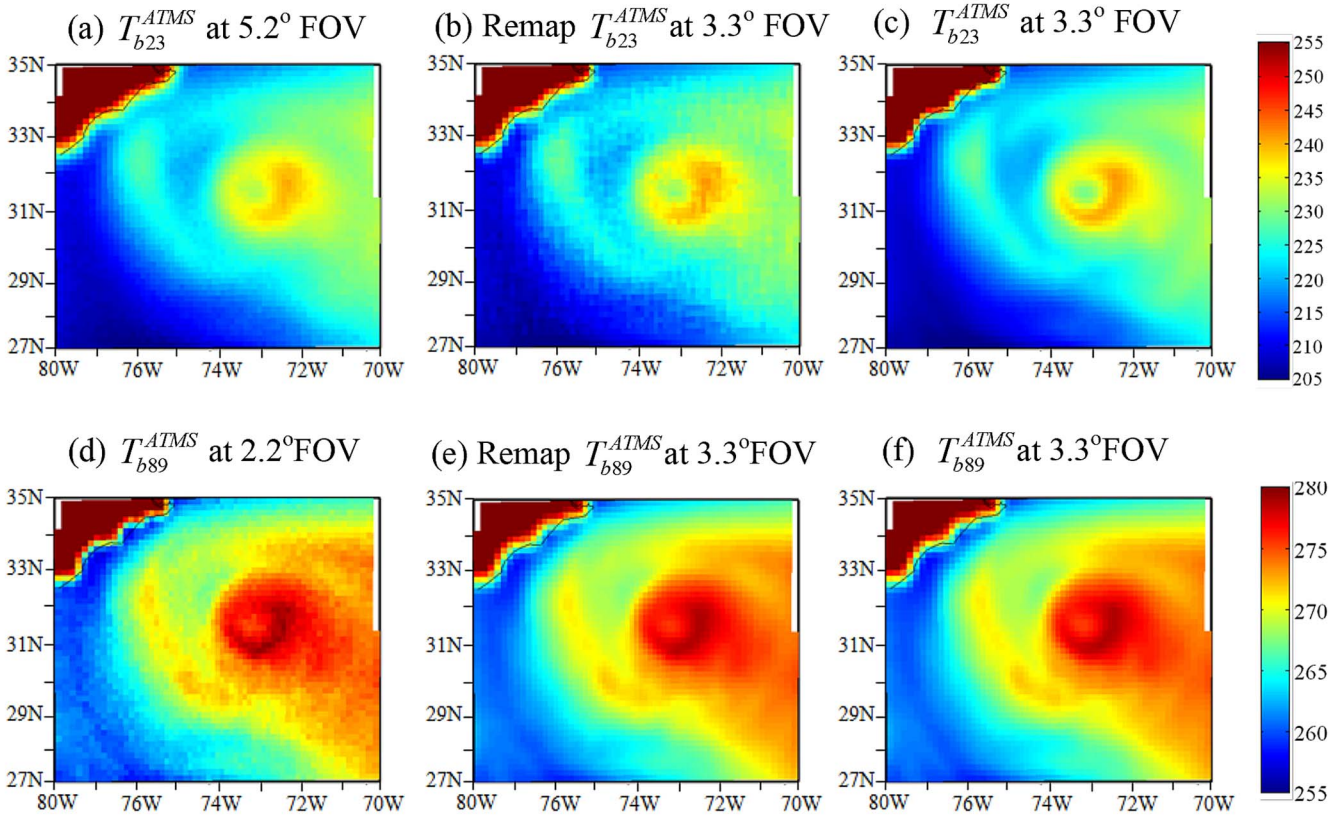

Fig. 3. (Left) Model simulated brightness temperature observations for the original FOV size, (middle) the remapped observations at expected FOV size, and (right) "real" observations at expected FOV size for (a)–(c) channel 1 and (d)–(f) channel 16. (a) T_{b23}^{ATMS} at 5.2° FOV. (b) Remap T_{b23}^{ATMS} at 3.3° FOV. (c) T_{b23}^{ATMS} at 3.3° FOV. (d) T_{b89}^{ATMS} at 2.2° FOV. (e) Remap T_{b89}^{ATMS} at 3.3° FOV. (f) T_{b89}^{ATMS} at 3.3° FOV.

one (e.g., AMSU-A). In this paper, 3 × 3 data size was chosen for ATMS channels of 5.2° beamwidth, and 5 × 5 data grid was chosen for ATMS channels of 2.2° beamwidth. The other two parameters that need to be specified are w and γ. The parameter w is simply a scale factor to ensure the two terms in (5), i.e., Q_0 and $\Delta T_{\mathrm{rms}}^2$, are of the same magnitude but is otherwise arbitrary. The remapping coefficients from the B–G algorithm are independent of the precise choice of w [9]. In this paper, a constant value of 0.001 is given to w.

The B–G algorithm only provides a mathematical solution to the remapping problem. In order to make the solution applicable to the real ATMS brightness temperature measurements, an "optimal" selection of the γ value is such that when the coefficients are applied to uniform scenes, the reconstructed scene

brightness temperature of the FOV should remain the same as the raw observations. Therefore, an additional constraint

$$\sum_{i=1}^{n}\sum_{j=1}^{m} a_{ij} = 1 \tag{8}$$

is imposed to determine the "optimal" γ value. The B–G coefficient thus obtained not only guarantees that the reconstructed antenna pattern matches the target antenna pattern but also ensures that the reconstructed scene brightness temperatures are physically meaningful.

The third adjustable parameter in (7) is γ. When $\cos(\gamma)$ is equal to 0, the solution of (7) for the B–G coefficients becomes $1/G$, i.e., the reconstruction is simply the average of the raw observations. When $\cos(\gamma) = 1$, the solution derived from (7) takes a highly nonuniformly distributed value, which makes the reconstructed observations become most noisy. Therefore, the value of $\cos(\gamma)$ between 0 and 1 determines the tradeoff between resolution enhancement and noise reduction in the reconstructed fields. As shown in Fig. 2, the "optimal" value of γ is not only different for resolution reduction and enhancement but also different at different scan positions. For resolution enhancement (from 5.2° to 3.3° beamwidth), the optimal value of γ that satisfies (8) is around 0.1×10^{-3}, which is much smaller than the value of $\gamma = 0.1$ for resolution reduction (from 2.2° to 3.3° beamwidth). In implementing the B–G algorithm, the γ value needs to be determined case by case at every single scan position because the B–G coefficients are very sensitive to γ.

III. Evaluation of ATMS Remapping Results by Using Simulated Data Sets

When the FOV size of the remapped ATMS observations is made consistent with that of AMSU, the noise characteristic could be altered by the remapping process. Since the remapped ATMS observations are intended for numerical weather prediction (NWP) and climate change applications, a quantitative evaluation of noise characteristic of the remapped data set is highly expected by the user community. In this paper, such an evaluation is first carried out by using model-simulated data sets, which can be generated at any assigned FOV size with any given noise level. In the following, details about the generation of simulated ATMS observations at different channels and FOV sizes using the community radiative transfer model (CRTM) developed in NOAA [13] are described, and biases and noise characteristics in the remapped data sets are presented. It will be shown that an evaluation using model simulations is clear and straightforward since the truth is known.

The ATMS observations for Hurricane Sandy at 0600 UTC October 28, 2012 are simulated. The actual FOV size, sampling rate, and scan geometry of ATMS are considered. The surface and atmosphere geophysical parameters needed by CRTM are the 66-h forecast from the Hurricane Weather Research and Forecasting (HWRF) model. The HWRF forecasts are available within a rectangular domain (34.5° N, 40.38° N; 76.58° W, 69.62° W) at a grid resolution of 0.06°. First, an ATMS swath was generated by a simulation model incorporating the ATMS instrument scan geometry. The simulated swath is located within the HWRF model. A total of 50 scan lines were generated, with 96 FOVs for each scan. At each of 96 FOV positions, the main beam of the antenna pattern was divided into a subbeam interval at a resolution corresponding to the 0.06° grid resolution of HWRF. The scene brightness temperature $T^b(\hat{\rho})$ was calculated at each HWRF model grid using CRTM. Then, the antenna temperature $T^a(\hat{\rho}_0)$ at each FOV "measured" by ATMS can be derived from (3) by convolution of $T^b(\hat{\rho})$ with the projected antenna pattern $G(\hat{\rho})$. Finally, noise is added based on the NEDT value for each channel. Specifically, the noise is a Gaussian distribution with a standard deviation being set to the noise measured for that channel. Note that no noise is added to the "truth," which is the scene simulated at the expected FOV size. In this way, the absolute value of noise variation that arises from the remapping algorithm can be accurately determined by comparing the remapped "observations" with the scene "truth".

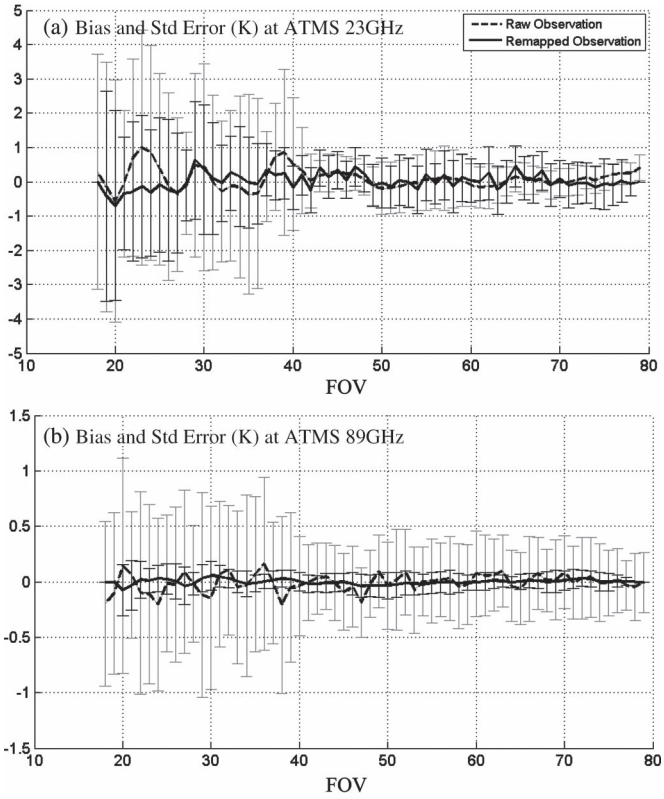

Fig. 4. Biases and standard deviations for ATMS observations before and after the remapping process for scan positions from 18 to 78 for ATMS channels 1 and 16. Solid curve and deep dark error bars are for the remapped observations, and dashed curve and light gray error bars are for the original observations. (a) Bias and standard error (K) at ATMS 23 GHz. (b) Bias and standard error (K) at ATMS 89 GHz.

TABLE I
Biases and RMS Errors for the Raw and the Remapped ATMS Observations at Channels 1 and 16

	ATMS Channel 1		ATMS Channel 16	
	Bias (K)	rms error (K)	Bias (K)	rms error (K)
Raw T_b^{ATMS}	0.10	1.32	-0.008	0.47
Remap T_b^{ATMS}	0.01	0.94	-0.007	0.09

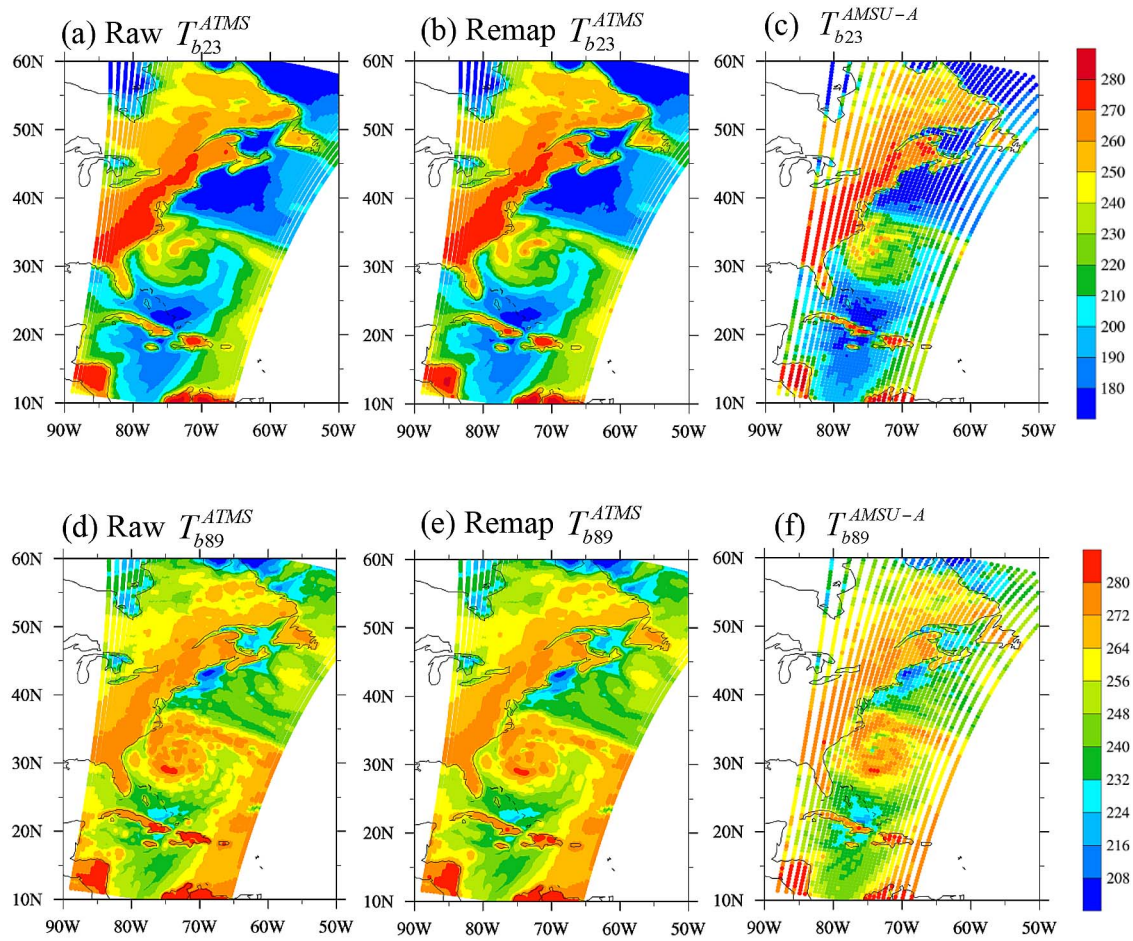

Fig. 5. (left) Raw ATMS, (middle) remapped ATMS, and (right) AMSU-A observations for Hurricane Sandy on October 28, 2012 for channels at (a)–(c) 23 GHz and (d)–(f) 89 GHz. (a) Raw T_{b23}^{ATMS}. (b) Remap T_{b23}^{ATMS}. (c) $T_{b23}^{\mathrm{AMSU\text{-}A}}$. (d) Raw T_{b89}^{ATMS}. (e) Remap T_{b89}^{ATMS}. (f) $T_{b89}^{\mathrm{AMSU\text{-}A}}$.

The simulation results at ATMS channels 1 and 16 are presented in Fig. 3. For channel 1, simulations are carried out for both 5.2° and 3.3° beamwidths. For channel 16, antenna temperatures are simulated for both 2.2° and 3.3° beamwidths. These simulations are used as the "truth". The B–G remapping coefficients are then calculated using the method described in Section II. The simulations with the 3.3° beamwidth were then used as "observation truth" to evaluate the remapping results for both channels 1 and 16. From Fig. 3, it is seen that even for the same channel, "observations" of different FOV sizes are quite different, particularly for those pixels within which the scene temperatures are inhomogeneous. For both cases, the remapped observations approximate very well the "truth". The remapped observations have larger noise, for channel 1, which corresponds to a resolution enhancement. For resolution reduction of channel 16, the remapped observations are smoother.

To quantitatively evaluate the noise change arising from the remapping algorithm, bias and root-mean-square (RMS) error at different scan positions for both the original and remapped observations were computed (Fig. 4). For a perfect remapping process, the remapped observations shall have no bias, and the RMS error shall be smaller than the channel sensitivity. Values of the bias and RMS error for observations before and after the remapping process are provided in Table I. For both channels, the RMS error of remapped observations is smaller than that in the raw observations. In other words, the consistency of FOV size between remapped observations and the scene "truth" reduces the bias. It is pointed out that the bias and RMS error of the remapped observations represent the data quality of remapped data sets. For channel 1, the RMS error is increased from a 0.25 K channel noise to 0.94 K due to a resolution enhancement, whereas a small bias around 0.1 ± 0.7 K exits in the remapped observations. For a resolution reduction of channel 16, the RMS error after remapping is 0.1 K, which is smaller than the 0.3 K channel sensitivity. The remapping process introduces no bias.

In summary, the bias arising from FOV differences was decreased after remapping. Improvements in spatial resolution can be achieved without increasing significantly the noise for resolution enhancement. For resolution reduction, the remapped results are of better quality with improved channel noise characteristics. In next section, the same B–G coefficients will be applied to the real observations of ATMS. The remapping results will be evaluated by real observations from NOAA-18 AMSU-A instrument.

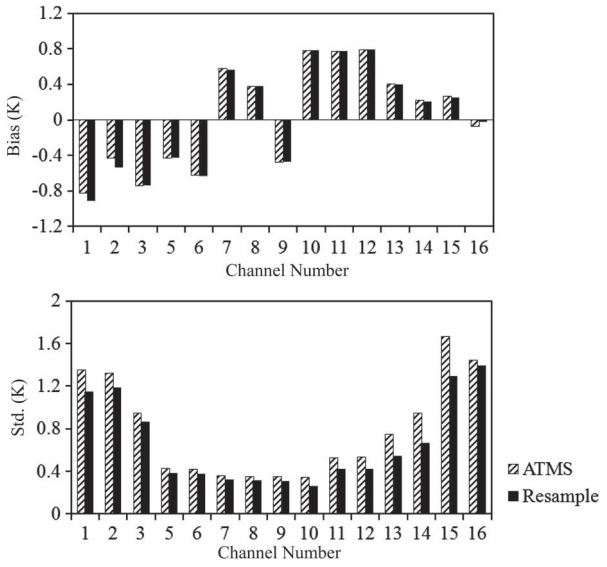

Fig. 6. Biases and standard deviations of the raw and remapped ATMS observations at channels 1–3 and 5–16.

IV. Evaluation of Remapping Results for Real Observations

Remapping the real measurements is very similar to remapping the simulated data set. Fig. 5 shows the raw observations and remapping results of ATMS channels 1 and 16 for Hurricane Sandy at 0600 UTC October 28, 2012. For comparison, AMSU-A observations are also provided in Fig. 5. For both channels, the remapped observations have a 3.3° beamwidth, which is the same as that of AMSU-A.

Evaluation of remapping results was carried out by using the simultaneous nadir overpass (SNO) method [14]. The spatial and temporal separations between ATMS and NOAA-18 AMSU-A FOVs are less than 15 km and 60 s. There are a total of 922 SNO data samples from ATMS and NOAA-18 AMSU-A during the time period from January 1, 2012 to March 31, 2013. A quality control is applied to remove outliers as those raw ATMS observations T_b^{Raw}, which deviate from the corresponding AMSU-A observation $T_b^{\mathrm{AMSU\text{-}A}}$ by more than Z times the biweighted standard deviation $\mathrm{STD_{bw}}$ from the biweighted mean difference $\mu_{\mathrm{bw}} = \overline{T_b^{\mathrm{Raw}} - T_b^{\mathrm{AMSU\text{-}A}}}^{\mathrm{bw}}$ [15], i.e.,

$$\frac{T_b^{\mathrm{Raw}} - T_b^{\mathrm{AMSU\text{-}A}} - \mu_{\mathrm{bw}}}{\mathrm{STD_{bw}}} \geq Z \tag{9}$$

where Z is called the Z-score. In this paper, Z is set to be 2 for all channels. After quality control, there remain 550 data samples for analysis.

Based on the SNO data, biases and standard deviations at ATMS channels 1–16 were computed for both raw and remapped observations at these channels, except for ATMS channel 4, for which there is no corresponding AMSU-A observations. As shown in Fig. 6, compared with the original observations, the biases are almost the same, but standard deviations are significantly reduced after the remapping process. These results are consistent with those derived from simulated data sets. It should be noted that, since the data samples used to carry out the evaluation are all from observations at nadir, the biases and standard deviations at other scan positions may be different. In addition, the geolocation mismatch and differences of calibration accuracy between ATMS and AMSU may also have some impacts on the results of evaluation.

V. Summary and Conclusion

Numerical results from simulated data sets and real satellite observations show that the B–G remapping algorithm can be effectively used to produce AMSU-A-like ATMS observations. Decreasing the brightness temperature difference stemming solely from spatial resolution differences, the RMS scale, according to Table I in Section III, is about 37% for ATMS channels 1 and 2 and 81% for channels 3–16. The random noise is increased by 0.6 K for channels 1 and 2 by the remapping. However, the channel sensitivity is improved for other channels by the remapping. The B–G algorithm takes advantages of the oversampling characteristic of ATMS channels 1–16 and generates a set of observations at different frequencies with enhanced or reduced spatial resolutions. For channels that involve a resolution enhancement, the remapping products could better resolve small-scale features that would otherwise be lost. This could be important for improved satellite retrievals of atmospheric quantities such as warm core structures in tropical cyclones.

Future work will focus on the remap of ATMS channels 1–16 observations to a set of arbitrarily chosen FOV sizes to optimize ATMS data applications in NWP models with different resolutions.

References

[1] "Advanced Technology Microwave Sounder (ATMS) SFR Radiometric Calibration Algorithm Theoretical Basis Document (ATBD)," Center Satellite Appl. Res. Nat. Center Weather Clim. Prediction, College Park, MD, USA, Doc. No: D43751 Rev C, 2010.

[2] *NOAA KLM User's Guide, Section 3.3*, National Oceanic Atmospheric Administration, Washington, DC, USA, Apr. 2007.

[3] F. Weng, X. Zou, X. Wang, S. Yang, and M. D. Goldberg, "Introduction to Suomi national polar-orbiting partnership advanced technology microwave sounder for numerical weather prediction and tropical cyclone applications," *J. Geophys. Res.*, vol. 117, no. D19, pp. D19112-1–D19112-14, Oct. 2012.

[4] F. Weng, K. Wang, and X. Zou, "30-Year atmospheric temperatures derived from satellite microwave sounding instruments using a 1D-Var approach," *J. Clim. Res.*, to be published.

[5] C. Zou and W. Wang, "Intersatellite calibration of AMSU-A observations for weather and climate applications," *J. Geophys. Res.*, vol. 116, no. D23, pp. D23113-1–D23113-20, Dec. 2011.

[6] C. A. Mears, F. J. Wenze, P. Thorne, and D. Bernie, "Assessing uncertainty in estimates of atmospheric temperature changes from MSU and AMSU using a Monte-Carlo estimation technique," *J. Geophys. Res.*, vol. 116, no. D8, pp. D08112-1–D08112-16, Apr. 2011.

[7] C. A. Mears and F. J. Wentz, "Construction of the remote sensing systems V3.2 atmospheric temperature records from the MSU and AMSU microwave sounders," *J. Atmos. Ocean. Technol.*, vol. 26, no. 6, pp. 1040–1056, Jun. 2009.

[8] A. Stogryn, "Estimates of brightness temperatures from scanning radiometer data," *IEEE Trans. Antennas Propag.*, vol. AP-26, no. 5, pp. 720–726, Sep. 1978.

[9] W. D. Robinson, C. Kummerow, and W. S. Olson, "A technique for enhancing and matching the resolution of microwave measurements from the SSM/I instrument," *IEEE Trans. Geosci. Remote Sens.*, vol. 30, no. 2, pp. 419–427, May 1992.

[10] M. R. Farrar and E. A. Smith, "Spatial resolution enhancement of terrestrial features using deconvolved SSM/I microwave brightness temperatures," *IEEE Trans. Geosci. Remote Sens.*, vol. 30, no. 2, pp. 349–354, Mar. 1992.
[11] D. G. Long and D. L. Daum, "Spatial resolution enhancement of SSM/I data," *IEEE Trans. Geosci. Remote Sens.*, vol. 36, no. 2, pp. 407–417, Mar. 1998.
[12] R. Sethmann, B. A. Burns, and G. C. Heygster, "Spatial resolution improvement of SSM/I data with image restoration techniques," *IEEE Trans. Geosci. Remote Sens.*, vol. 32, no. 6, pp. 1144–1151, Nov. 1994.
[13] Y. Han, F. Weng, Q. Liu, and P. V. Delst, "A fast radiative transfer model for SSMIS upper atmosphere sounding channel," *J. Geophys. Res.*, vol. 112, no. D11, pp. D11121-1–D11121-12, Jun. 2007.
[14] C. Cao, F. Weng, M. D. Goldberg, X. Wu, H. Xu, and P. Ciren, "Intersatellite calibration of polar-orbiting radiometers using the SNO/SCO method," in *Proc. IEEE IGARSS*, 2005, pp. 109–112.
[15] X. Zou and Z. Zeng, "A quality control procedure for GPS radio occultation data," *J. Geophys. Res.*, vol. 111, no. D2, pp. D02112-1–D02112-13, Jan. 2005.

Hu Yang (M'09) received the Ph.D. degree from the Chinese Academy of Sciences, Beijing, China, in 2003.

During 2003–2011, he was a Senior Research Scientist with the National Satellite Meteorological Center, China Meteorological Administration, leading the microwave instrument calibration and satellite ground application system development as Instrument Scientist and Program Scientist. In 2012, he joined the Earth System Science Interdisciplinary Center, University of Maryland, College Park, MD, USA, working on NPP/JPSS satellite calibration/validation as Project Principal Investigator. He has published more than 40 peer-reviewed journals. His main study field includes passive microwave radiometer calibration/validation, satellite geolocation, 1D-Var retrieval, and satellite observation simulation.

Dr. Yang was the recipient of the 2010 National Defense Science Advancement Award from the China Aeronautic and Space Agency for his outstanding contribution to the development of China's first spaceborne microwave imager radiometer.

Xiaolei Zou received the Ph.D. degree from the Chinese Academy of Sciences, Beijing, China, in 1988.

She is currently a Professor with the Department of Earth, Ocean and Atmospheric Science, Florida State University (FSU), Tallahassee, FL, USA. During 1989–1993, she developed the 4D-Var system of the National Meteorological Center (now the National Centers for Environmental Prediction) medium-range forecast model with full physics. She was a Scientist at the National Center for Atmospheric Research (NCAR), where she developed MM5 4D-Var system and worked on GPS radio occultation data assimilation ever since. After four years (1993–1997) at NCAR, she returned to FSU in 1997 to become a Professor with the Department of Earth, Ocean and Atmospheric Science and worked mainly on satellite data assimilation and their applications to hurricane forecasts and climate prediction studies. She has published over 80 papers in peer-reviewed journals.

Dr. Zou was the recipient of the 2008 AMS Fellow Award for her outstanding contributions to the applications of satellite data in the numerical weather prediction models and education in data assimilation.